ACCEPTED MANUSCRIPT

Highly Sensitive 3C-SiC on glass based thermal flow sensor realized using MEMS technology

Vivekananthan Balakrishnan[a], Toan Dinh[a], Hoang-Phuong Phan[a], Dzung Viet Dao[b] and Nam-Trung Nguyen[a,*]

[a]*Queensland Micro- and Nanotechnology Centre, Griffith University, Brisbane, QLD 4111, Australia*

[b]*School of Engineering, Griffith University, Gold coast, 4222, QLD, Australia*

* *nam-trung.nguyen@griffith.edu.au*

Research Highlights

- Thermoresistive properties of a Cubic Silicon carbide (3C-SiC) on glass sensor are studied. The negative temperature coefficient leads to an increasing signal with increasing flow velocity.
- The relationship between the geometry of the SiC heater and the sensor performance is studied. A larger heater leads to a higher sensitivity.
- Influence of flow direction on the sensor performance was studied. Downstream sensor is more sensitive.
- The developed SiC thermal flow sensor combines the advantages of simplicity, low power consumption, high sensitivity and full dynamic range of air flow.

Abstract:

This paper presents a silicon carbide (SiC) based thermal flow sensor on a transparent and electrically insulating glass substrate via anodic bonding process. The paper elaborates on the fabrication steps of the thermal flow sensor. Three resistive heater size configurations of dimensions 100µm × 100µm, 300µm × 300µm, and 1000µm ×1000µm were fabricated. The thermoresistive properties of 3C-SiC on glass were investigated from ambient temperature to 443K. The characterization of the SiC heater and temperature sensors revealed a high thermoresistive effect with a temperature coefficient of resistance (TCR) of approximately -20716ppm/K at ambient temperature(298K) and -9367ppm/K at 443K respectively. The performance of the sensors was evaluated based on the sensitivity of the flow sensor. For a turbulent flow velocity of 7.4m/s, the sensitivity of the sensor operating in the constant -voltage mode is 0.091s/m with a power consumption of 133.50mW for the 1000µm ×1000µm heater. Finally, a study on the flow direction was conducted to confirm the operation of 2-D direction independent hot-film flow sensor. Results indicated that the performance of the sensor remained the same when the flow direction was perpendicular to SiC heater and sensor respectively. However, the best sensitivity was achieved by passing air flow perpendicular to the sensing elements. The high TCR of the single crystalline 3C-SiC material, the relatively low power consumption on the order of milliwatts and the high sensitivity of our sensor demonstrates its potential use for high temperature flow sensing applications

Keywords: SiC flow sensor, glass, thermoresistive effect, air flow, sensitivity

1. Introduction

Microelectromechanical systems (MEMS) based sensors have been rapidly emerging in recent years due to the effective utilization of various physical phenomena such as thermoresistive, thermoelectric and piezoresistive effects[1,2]. Due to the simplicity and high sensitivity of thermoresistive sensors, thermoresistive effect has been the main transduction mechanism for many thermal sensing[3].Thermoresistive effect refers to the change in electrical resistance with temperature variation. Thermoresistive devices for sensing flow[4–8], temperature[9–11],acceleration[12,13] and inertial[14,15]applications have been reported in the literature. Among these physical parameters, flow rate and flow velocity are required in many applications such as aerospace[16], chemical process

ACCEPTED MANUSCRIPT

control[17],deep-sea exploration[18,19] and automotive systems[16]. These applications in a harsh environment typically operate at a temperature between 300°C-550°C and thus require highly reliable and sensitive sensing materials. More importantly, high stability, fast response time, low power consumption and cost effectiveness are important for the selection of device material.

Recently,our research group has reported an extensive review on the thermoresistive effect in metals and semiconductors,design considerations and applications to provide an insight for industrial designers and researchers around the globe[20]. As a result, the choice of materials for developing a thermal flow sensor depends on its sensing performance and the applications. A large temperature coefficient of resistance (TCR) is desirable for a highly sensitive thermal flow sensor. Among the available sensing materials, nanocomposites and ceramics exhibit huge thermoresistive effect, i.e. large TCR of up to 10^{12}ppm/K were employed as temperature sensing elements. As these materials have a high resistivity, they are not suitable for thermal flow sensors which primarily operate based on Joule heating. To increase the temperature of the heater at low supply voltage or current, a relatively low resistivity (i.e in the range of 10^{-1} -10^{-6}Ωcm is required. Therefore, in the last two decades the materials for this purpose have been metals (e.g platinum, nickel) and highly doped semiconductors (Si, Ge). For instance, platinum with resistivity from10^{-4} -10^{-6}Ωcm and a highly doped silicon with resistivity10^{-1} -10^{-2}Ωcm have been utilized in microheater devices. However, these materials posses a low thermoresistive sensitivity (i.e lesser than 5000ppm/K) thereby requiring a novel and unprecedented material for wide range of thermal sensing applications.

Due to the excellent physical,electrical,mechanical and chemical properties[21–23] SiC based MEMS sensors have attracted great attention for thermal flow sensing applications[24–27]. Among over 250 polytypes of SiC, 3C, 4H and 6C are the most well-known crystals.Unlike the 4H and 6C-SiC polytypes, 3C-SiC can be heteroepitaxially grown on Si substrates by Liquid Pressure Chemical Vapor Deposition (LPCVD) process. Heteroepitaxy is possible because 3C-SiC and Si have similar cubic structures with a lattice mismatch of approximately 20%. This growth process overcomes the large lattice mismatch by carbonization, a process used to form thin 3C-SiC film directly on Si substrates resulting in SiC/Si heterojunction to establish good electrical insulation[28].As a result, it offers the advantage of batch fabrication since high quality and large area Si substrates are readily available at low cost [29,30]. Furthermore, 3C-SiC grows at low temperature while hexagonal polytypes (4H and 6C) needs high growth temperature due to differences in the energy of formation[31].

However, the commonly employed SiC on Si system has a few drawbacks. For instance, Si becomes conductive over 200°C resulting in current leekage between SiC and Si. In addition, the yield strength of Si reduces beyond 450°C. Therefore, the fabrication of devices in these layers requires high electrical isolation. Unlike poly-SiC, 3C-SiC cannot be grown directly on glass or any other non-conducting sacrificial material , thereby making surface micromachining and electrical isolation of single crystalline 3C-SiC structures very difficult. In the last few years, a number of efforts have been made to transfer SiC on to an insulating substrate. Cioccio et al demonstrated the possibility of using Smart cut process which combines ion implantation with wafer bonding to form SiC on insulator(SiCOI)structures.However, this technique suffers from implantation damage and the stress issues with large Si wafers[32]. Other bonding techniques reported in[33–35] have relied on diffusion bonding to transfer SiC onto an insulator substrate. Moreover, the bonding process was complex, as it requires an ultrasmooth buffer layer such as glass formed by sputtering/oxidation. As a result, we have been motivated to find alternate methods for producing SICOI structures. Recently, our research group has reported a new platform to create SIC on an electrically insulating and transparent substrate using anodic bonding process for bio-sensing applications[36]. As a result, this technique has been employed to fabricate the thermal sensor structures for MEMS flow sensing applications.

2. Experimental

2.1 Fabrication technology

The fabrication of micro flow sensor involves seven processing steps beginning with the growth of single crystalline 3C-SiC thin films on Si substrate. Figure 1 depicts the process flow of SiC temperature sensors and heaters. SiC films were heteroepitaxially grown on a 6 inch Si substrate in a hot-wall low pressure chemical vapour deposition reactor. The Si wafers were then subjected to RCA cleaning prior to the growth of SiC to remove the surface contaminants. The epitaxy growth process employed silane and propylene as the silicon and carbon containing sources at 1000°C[37]. The deposited SiC film was found to be n-type doped due to the presence of nitrogen residual gas. The Atomic force microscopy (AFM) data revealed the surface roughness of the films to be 7nm, which is sufficient for anodic bonding technique[36].

ACCEPTED MANUSCRIPT

During this process, the SiC/Si bonding to glass (6 in. 1-mm-thick Borofloat 33 from University Wafers, South Boston, United States) was performed in an EVG520IS hot embosser at a maximum pressure of 137kPa and a bias voltage of 1000V, Figure 1(a). The chemical bonding between SiC and glass substrate was established by applying cathode electrode to glass wafer and anode electrode to SiC/Si wafer, respectively. As a result, the cathode attracted the positive charges in the glass wafer, thereby leaving a depletion layer at the SiC/glass interface. Consequently, the negative charges were repelled by the cathode and move towards the anode and diffused into SiC to form bonding. Using X-ray Photoelectron Spectroscopy (XPS) technique, the fabricated SiC/glass wafer was surface characterized with sharp bonding. In addition, Raman spectroscopy showed good crystallinity in the wafer. Finally, a pulling test on the bonded device was conducted to determine the adhesion strength. The measured tensile strength of 20MPa suggested the capability of SiC on Si (SiCOI) platform for high-temperature electronic and sensing applications.

Next, the silicon layer was removed by mechanical polishing and subsequent wet etching. During the first step, the top Si layer was polished by applying a maximum pressure of approximately 170kPa to the Si/SiC/glass sample. The rotational speed was set at 40rpm and the Si removal rate was measured as 10 μm/min with calcined aluminium oxide powder. Furthermore, a mixture of $HF, HN0_3$ and CH_3COOH with a ratio of 2:2:3 was employed to wet etch the remaining Si to form SiC on glass wafers, Figure 1(b).

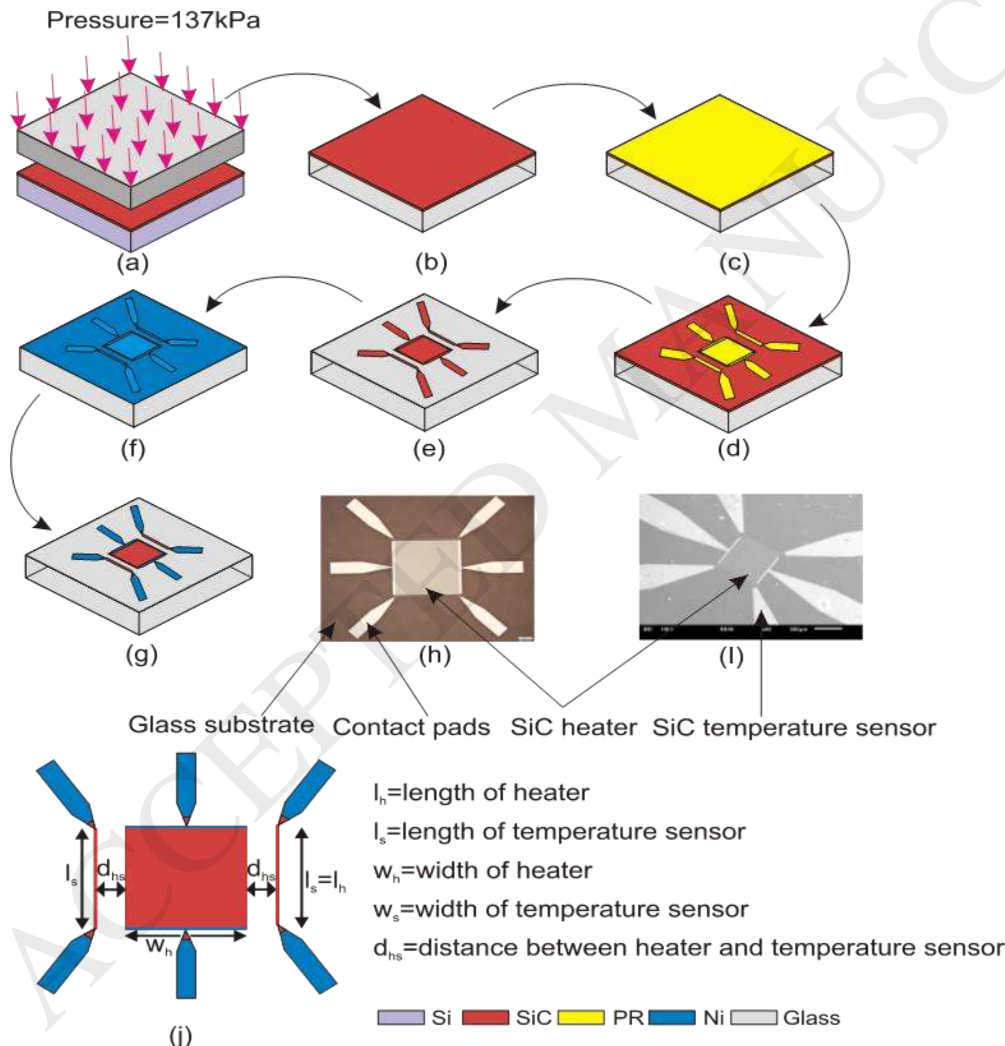

Figure 1. Fabrication process flow of SiC temperature sensors and heaters on a glass substrate, **(a)** Bonding of SiC/Si on glass; **(b)** Si removal to form SiC on glass; **(c)** Photoresist (PR) coating; **(d)** PR patterning; **(e)** Etching SiC; **(f)** Ni deposition; **(g)** Ni etching; **(h)** Photographic image of the SiC thermal sensor; (i) Scanning Electron Microscope (SEM) image of the SiC/glass thermal sensor; (j) Geometric sketch of the SiC thermal sensor

The bonding process is followed by coating the photo resist and photolithography, Figure 1(c). Then, the SiC layer was patterned using ICP plasma etching process, which employed hydrogen chloride and oxygen as the

ACCEPTED MANUSCRIPT

active gases, Figure1(d). The etching mask for SiC was a 1.2µm thick AZ6612 photoresist with a etch rate of approximately 100nm/min, Figure 1(e). Next, nickel electrodes were deposited on the SiC/glass wafer by sputtering, Figure 1(f). The final step involved in patterning the Ni electrodes by removing the lift-off photoresist, Figure 1(g). Figure 1(h),1(i) and 1(j) depict the photographic image, SEM image and the geometrical sketch of the fabricated thermal sensor. Three different heater sizes were fabricated using the above fabrication process. The width(w_s) of SiC temperature sensors and the distance between heater and sensors(d_{hs}) is 10µm for all three configurations, Figure1(j). The thickness of the heater and the sensors measure 300nm. Table 1 lists the varying geometrical parameters of the three designs employed for flow characterization discussed subsequently. The sensor temperature-resistance dependency study was made on the largest heater of 1000µm ×1000µm. As the width and length of the SiC heating film are equal (1000µm× 1000µm), the sheet resistance ($R_s=\rho/t$) and the resistance are equal and calculated to be 258kΩ/sq. With a 300nm thick heating film, the electrical resistivity is calculated to be7.74Ωcm. Flow characterisation measurements were carried out on all three designs.

Table 1. Overview of the fabricated thermal sensors for flow measurement

Configuration number	1	2	3
Width of heater(µm)	100	300	1000
Length of heater(µm)	100	300	1000
Length of temperature sensor(µm)	100	300	1000
Width of temperature sensor(µm)	10	10	10
Distance between temperature sensor and heater(µm)	10	10	10

2.2 Experimental set-up

Figure 2(a) illustrates the experimental setup for investigating the thermoresistive effect. Before conducting the actual measurements in the flow channel, the SiC heater and temperature sensors were characterized with this setup. The thermal properties of the SiC thin-film resistors were studied by placing them on a hot-plate (TD-330F model, Thermoline Scientific). During the heating phase, the temperature was established by the controller of the hot plate. The actual temperature was monitored by a thermocouple (resolution of 1 K, accuracy of ±3%). With an equal interval of 15°C, the resistance change of upstream and downstream sensors were measured using two ohmmeters (QM 1535) and the current flowing through the heater was measured using an ammeter for calculating the heating power.

ACCEPTED MANUSCRIPT

ACCEPTED MANUSCRIPT

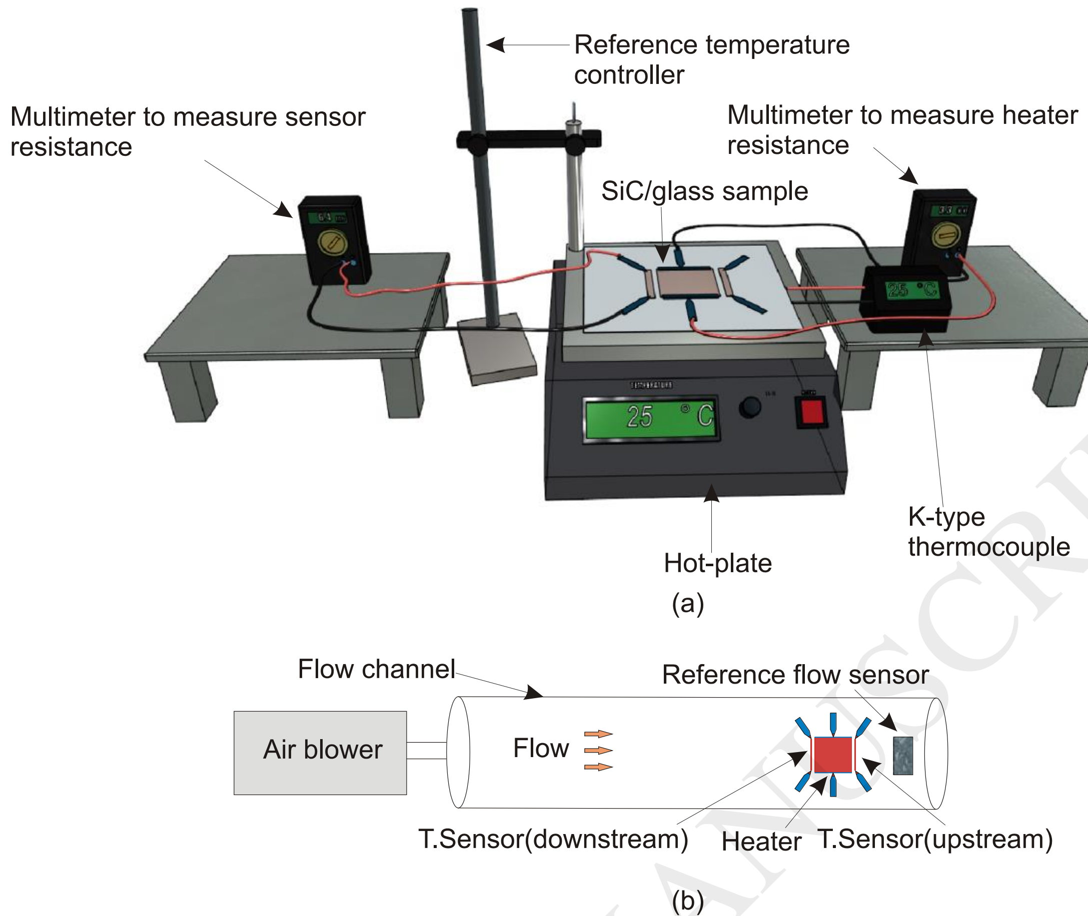

Figure 2. Schematic of the experimental setup: **(a)** Thermoresistive thin film characterization; **(b)** Flow response characterization

Figure 2(b) shows the experimental setup to demonstrate the flow sensing capability of our device. A Polyvinyl Chloride (PVC) pipe with a length of 15cm and an inner diameter of 5cm was employed as a flow channel. An air blower (LB0115-002, Industrial Equipment and Control) was utilized to generate air flow ranging from 0.2 to 9m/s at room temperature (23°C), while a hot wire anemometer (Testo450i wireless smart probe) was used as a reference flow sensor. The device was mounted at one end of the pipe and the air blower was positioned at the other end. The reference flow sensor was placed near the device and the flow rate was monitored by a Bluetooth based smart device. The heater was supplied with a constant voltage. The resistance change of the upstream and downstream sensors were measured using two Ohmmeters (QM 1535) at various air flow velocities for the three devices with different heater sizes (Table 1). A number of resistance values were recorded in both the absence and the presence of air flow and the mean values were used to plot the relative resistance change of the sensor, presented in the next section.

3. Results and discussions

3.1 Thermoresistive thin film characterization

During the thermal energy excitation, the number of free charge carriers in single-crystalline n-type SiC material increases with increasing temperature. Therefore, this leads to a decrease in electrical resistivity of the material indicating the negative temperature coefficient of resistance (NTC). However, the electron and hole mobility of the material decreases with the rise of temperature due to scattering effect of lattice vibrations[38]. Figures 3(a) and 3(b) depict the variation of heater resistance and sensor resistance respectively with temperature.

ACCEPTED MANUSCRIPT

ACCEPTED MANUSCRIPT

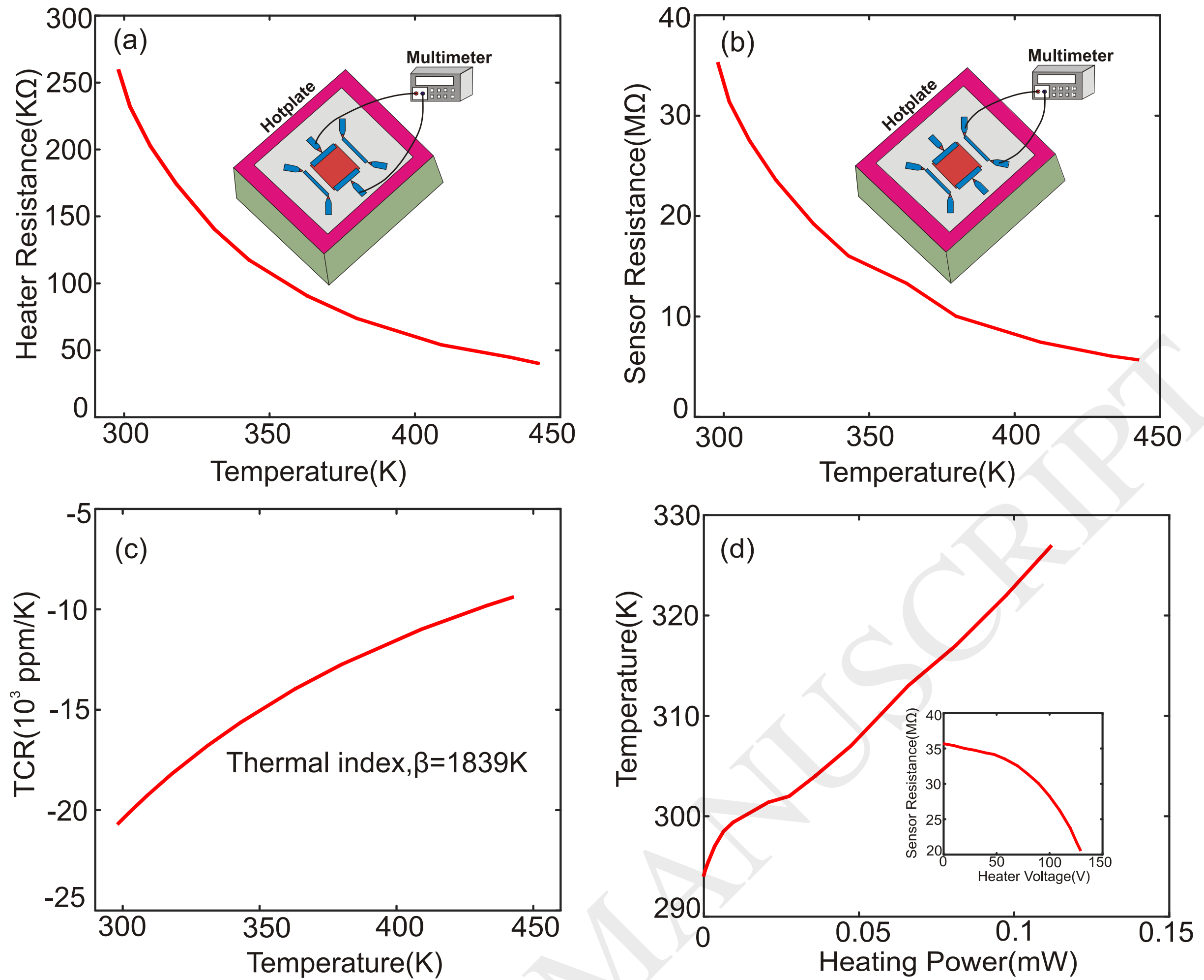

Figure 3. Thermoresistive characteristics of 3C-SiC on glass for design 3 **(a)** Heater resistance as function of temperature; **(b)** Sensor resistance as function of temperature. Inset shows the experimental setup; **(c)** TCR as a function of temperature; **(d)** Temperature as measured by the sensor as function the applied heating power. Inset shows the values of sensor resistance as function of the voltage applied on the heater

We observed that the resistance of heater and sensor significantly decreased by approximately 82% and 85% when the temperature increased from room temperature of 23°C to 170°C due to thermoresistive effect. During the cooling phase, the resistance of SiC on glass returned to its original value, thereby indicating a good reproducibility. The decrease in sensor and heater resistance at high temperatures indicate that the ionization of impurities dominate[36] ,leading to a higher carrier concentration. The temperature dependence of electrical resistance on n-type 3C-SiC can be characterised by the following expression:

$$R = R_o e^{\beta\left(\frac{1}{T}-\frac{1}{T_o}\right)} \tag{1}$$

Where T_o and T denote thermodynamic temperature at the beginning and end of measurement, R_o and R denote the resistance at temperature T and T_o respectively. β is thermal index which is used to evaluate the sensitivity of thermoresistive effect as an alternative parameter to TCR. The relationship between β and TCR (α) is given by

$$TCR = {}^{-\beta}\!/_{T^2} \tag{2}$$

Using equation (1), the thermal index β was evaluated to be 1839.7K which is comparable to the values reported in literature recently[39–41] The TCR(Figure.3c) of the transferred SiC film was estimated to range from -

ACCEPTED MANUSCRIPT

9367ppm/K (443K) to -20,716ppm/K (298K) which is comparatively higher than the metals[5][42], highly doped 3C-SiC[43,44], graphite inks[45], pencil graphite[46], graphene[47] and carbon-nano tubes(CNT)[48] based materials reported in literature. Moreover, it indicates the occurrence of a huge thermoresistive effect primarily required for the development of highly sensitive flow sensors. We also conducted an experiment to study the relationship between the sensor resistance and heating power that will aid in the fluid flow characterization thereafter. We observed that the sensor resistance decreases by 42% when the heater is biased from 0 to 130V as shown in the inset of Fig.3d. The heating power could be estimated as follows: $P_h=V_h^2/R_h$, where V_h and R_h are the voltage applied on the heater and heater resistance respectively. Figure 3(d) shows the relationship between the heating power and temperature of the sensor interpreted from Fig.3b. It is noteworthy that due to reduced heat loss into the glass substrate, only a heating power on the order of milliwatt is required, demonstrating the potential use for low-power thermal sensing applications.

3.2 Flow sensor Characterization

The configuration shown in figure 1(h) and (i) resemble calorimetric flow sensing. However, the working principle of our SiC/glass flow sensor is the same as that of conventional hot-film anemometer. That is, when a constant voltage is applied to the SiC heater, the temperature of heater increases as a result of Joule heating Phenomena[49,50]. As the air flow normal to the downstream temperature sensor increases, heat loss due to convection from the heater occurs along with the heat conduction to the glass substrate. However, the heat conduction is more dominant than the forced air convection, leading to decrease in temperature for both the sensing resistors. As the sensors exhibit the negative temperature coefficient of characteristics (NTC) shown in Fig.3C, the differential change in resistance follow an increasing trend. Figures 4(a), (b) and (c) shows the relative resistance change of the sensors with respect to heating power at a constant air flow velocity of 2.92m/s. As the heating power is geometry-dependent, each heater requires different heating power to show comparable resistance change during the flow. The relative resistance change is calculated as:

$$\Delta R/R = \frac{R_{\text{flow off}} - R_{\text{flow on}}}{R_{\text{flow off}}} \qquad (3)$$

where $R_{\text{flow off}}$ and $R_{\text{flow on}}$ represent the initial resistance prior to turning the air blower on and the resistance of a stable data shown on the Ohmmeter in the presence of the flow. The response of upstream (blue) and downstream (red) resistors are quite similar with a smaller increase in resistance change for downstream resistors for all configurations. This is due to the asymmetric temperature distribution around the heater. Due to forced convection, the downstream temperature is higher than the upstream temperature. For instance, the change in resistance accounts for 1.2%, 12% and 50% approximately for the designs 1, 2 and 3, respectively.

ACCEPTED MANUSCRIPT

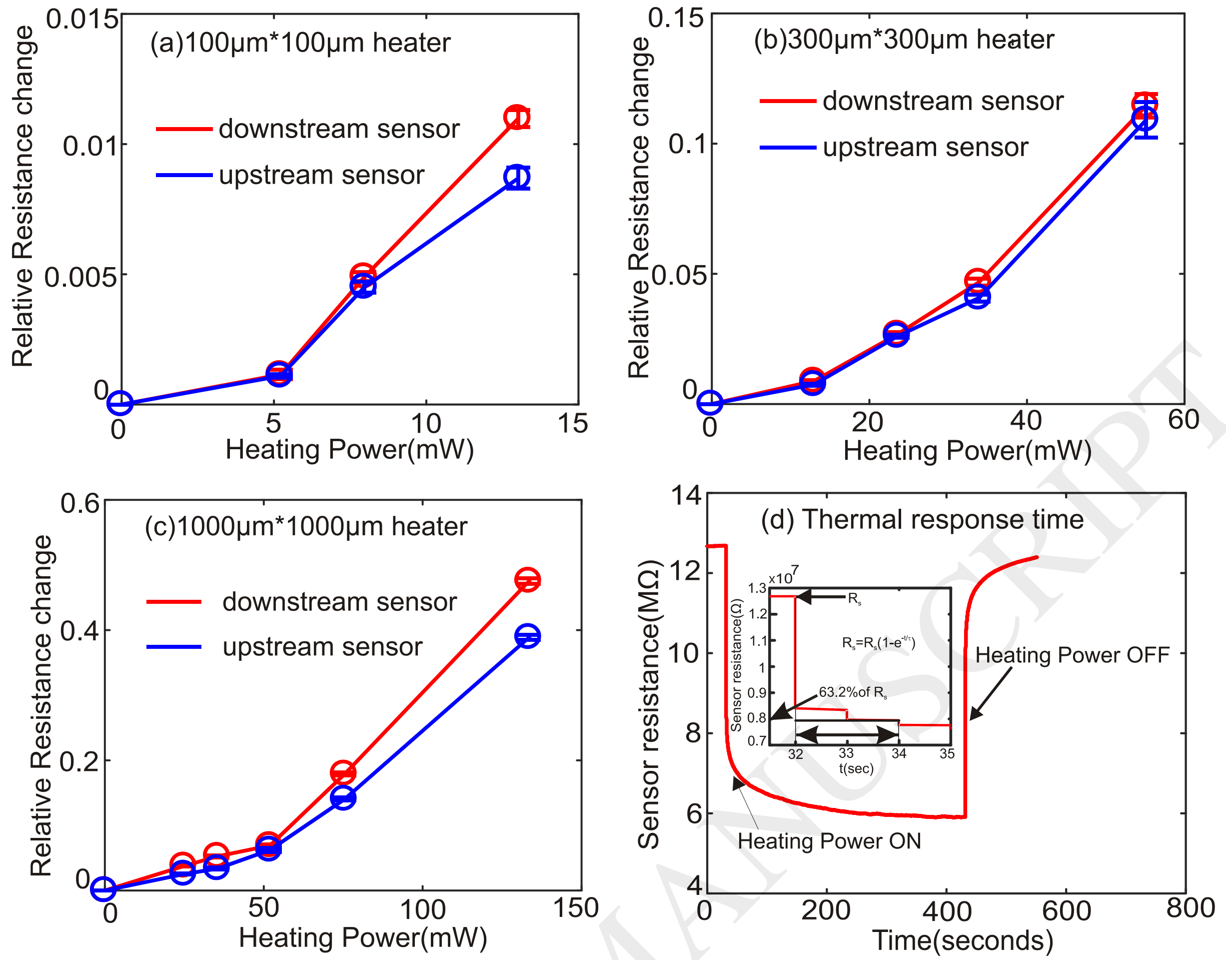

Figure 4. Performance of different heaters at constant air flow velocity of 2.92m/s when the air flow is perpendicular to temperature sensor, **(a)** 100µm × 100µm; **(b)** 300µm × 300µm; **(c)** 1000µm ×100µm; **(d)** Thermal response time indicating the heating and cooling transition for one cycle to a heating power of 55.2mW for 300µm ×300µm heater. Inset shows the zoomed in response to calculate the thermal time constant.

Figure 4(d) shows the thermal response time(TTC), a key feature that presents the capability to respond instantaneously to change in external signals such as temperature, flow etc. Assuming a first order model to our SiC thermal sensor, the time response is represented as $R_s(t)=R_o(1-e^{-t/\tau})$, where R_o represents the initial sensor resistance and τ represents the thermal time constant. Experimentally, it is defined as the time needed for the amplitude of the sensor output to reach 63% (1-1/e) of the steady-state signal. The sensor resistance was recorded using an ohmmeter over a period of time until it reached the steady-state during the heating and cooling phases. From the inset of fig.4(d), the response time was estimated to be approximately 2s, which is comparable to that of other thermal flow sensors made on a less thermally conductive substrate[31]. This response of SiC on glass platform is quite slower than the response time of various MEMS thermal sensor platforms reported in the literature[51,52], where the response time is within the *ms* range, corresponding to a bandwidth of the kHz range. This is due to the large thermal mass of the glass substrate which supports the SiC heating and sensing elements. Scientifically, thermal mass refers to the thermal capacitance or the heating capacity. Theoretically, the time constant (τ) is expressed as $R_{th} \times C_{th}$, where R_{th} and C_{th} are the thermal resistance and thermal capacitance of the sensor. Thermal resistance can be calculated by $R_{th} = L/{A \times \kappa}$ where L, A and κ are the length, area of cross section and thermal conductivity of the material respectively. Thermal capacitance can be calculated by $C_{th} = \rho \times V \times C_\rho$ where ρ, V and C_ρ represent the density, volume and heat capacity of the material. The high thermal capacitance of glass (8.37×10^5J/Kg/K) in the above relationship mean slow response time. Therefore, a common strategy to achieve fast thermal response time is to scale down the thermoresistive elements or it is recommended to isolate the SiC material from the glass substrate by etching glass to make cavities prior to bonding of SiC on glass.

ACCEPTED MANUSCRIPT

Beside the thermal response time, the thermoresistive sensitivity is another important feature of thermal flow sensor. It is defined as the ratio of relative resistance change to temperature variation and can be evaluated by TCR. The temperature detection during the flow could be very easy if the TCR is higher for the sensor material and vice-versa. For example, the thermal sensors proposed in[53,54] offers low thermoresistive sensitivity and so sensing temperature changes is very difficult. As a result, the relative resistance change $(\Delta R/R)$ is commonly converted into voltage (ΔV) change by a Wheatstone bridge circuit and amplified thereafter to observe the flow response. However, the high TCR from the figure 3(c) strongly suggests that the relative resistance change (%) could be easily observed for our sensor. Accordingly, We have measured the change in upstream and downstream sensors resistance directly via Ohmmeter and the real-time signal using a 2450 source meter respectively.

The behaviour of the sensor can be evaluated by first calculating the Reynolds number of our set-up as this number indicates the flow regime. The Reynolds number for the pipe can be expressed as

$$Re_D = {}^{DV_f}\!/_{\upsilon} \tag{4}$$

where D is hydraulic diameter of the pipe is 0.05m, V_f the air flow velocity(m/s) and υ the kinematic viscosity of air is 15.11×10^{-6}m^2/s at 20 °C respectively. Up to a Reynolds number of 2300, the flow in the pipe is laminar. For Re_D>2300 the flow enters a turbulent regime and the transitional flow regime occurs between $0.69<V_f<0.79$m/s for $2300< Re_D<2600$. According to equation (4), the threshold velocity where the laminar flow regime ends is 0.69m/s and Re_D is estimated to range approximately from 662 to 29,781for the flow range 0.2 to 9m/s. The high Reynolds number indicates that the flow passing the SiC on glass sensor was turbulent with velocity above 0.78m/s. Characterization of the sensors at very low speeds is challenging because the air blower loses linearity at low flow speeds. The minimum detectable flow (MDF) velocity using our experimental set-up depends on various factors such as (i) the hydraulic diameter of the pipe, (ii) the size of the sensor chip, (iii) the size of the Printed Circuit Board (PCB) employed to wire bond the thermal sensor and (iv) the size of the PMMA plate to integrate the chip and PCB together. We utilized a 0.05m diameter pipe to mount the sensor chip due to the bigger sizes of PCB and PMMA respectively. The lower bound of the flow velocity that can be generated was about 0.2m/s, below which speed fluctuations were observed. On the other hand, the upper limit of the flow velocity that can be readily generated was about 9m/s, above which the temperature of the air becomes hot causing instability.

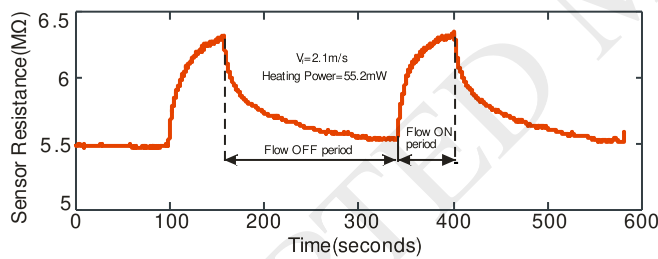

Figure 5. Real time sensor response for a heating power of 55.2 mW on 300µm×300µm heater

Fig.5 shows the real-time response of the sensor measured for design 2 (300µm×300µm) under a constant heating power of 55.2mW. It is evident that the relative resistance change $(\Delta R/R)$ was observed to be approximately 14% during the flow (V_f=2.1m/s) due to the cooling effect. The flow ON time, the time required for the signal from hot to cold transition is calculated to be 55s. The flow OFF time, the time required for the signal from cold to hot transition is approximately 3 minutes and this longer time strongly demonstrates the influence of glass substrate. The sensor resistance increased initially during the cooling phase and returned to an initial value during the heating phase indicating a very good reversible characteristics for all the two cycles.

In Figures 6 to 8, the sensor output characteristics were plotted over the air flow velocity in the channel for the three designs shown in table 1. The goodness of fit was obtained by polynomial curve fitting of order 2 with a high degree of accuracy. The R-squared value of quadratic fitting in figure.7a(heating power=23.64mW) is equal to 0.987 implying the fit explains 98.7% of the total variation in the data about the average. On the other hand, increasing the number of fitted coefficients in our model increased the R-squared value although the fit may not improve in a practical sense. The performance of the thermal sensor could be evaluated based on three different factors: (i) the amount of change in sensor resistance (%) due to perpendicular air flow (ii) the sensitivity (s/m) and (iii) the total relative standard error (%).

ACCEPTED MANUSCRIPT

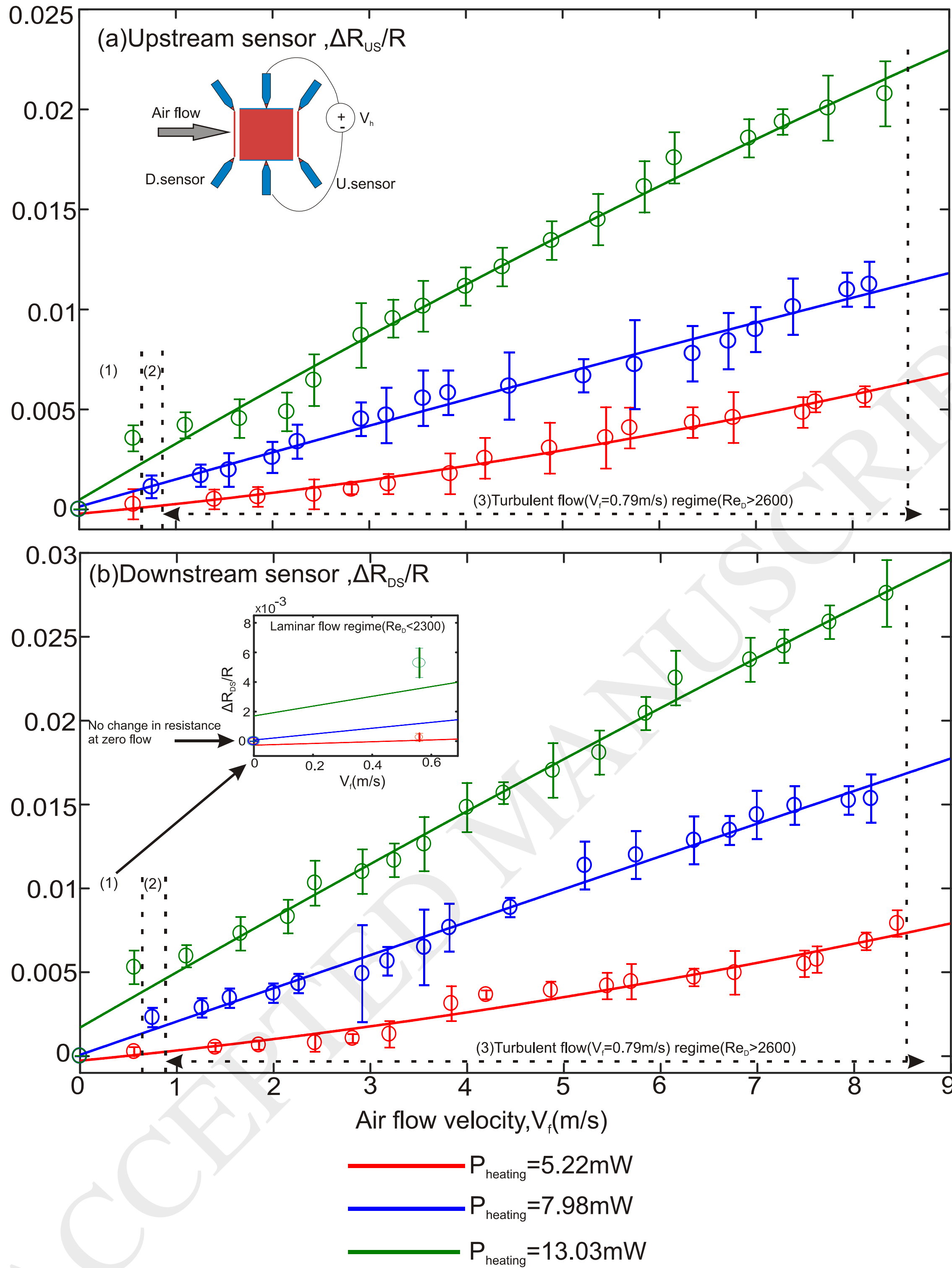

Figure 6. Performance of 100μm × 100μm heater with different supplied heating power when the air flow is perpendicular to temperature sensor, **(a)** upstream sensor; **(b)** downstream sensor. Inset of (a) shows the air flow direction and inset of (b) shows the zoomed in response under laminar flow regime.

We observed that higher heating power leads to larger change in relative resistance, and therefore higher sensitivity. For the smaller heater (100μm ×100μm), the downstream sensor resistance is changed by 0.76% (Fig. 6(a)), while the larger heater (1000μm ×1000μm) contributes to a huge change of 58.36% (Figure 8(a)) over a full range of flow. The characteristics of upstream sensor is similar to the downstream sensor despite a smaller resistance change. For instance, the resistance change reduces to 0.53% for the design 1 (Figure 6(b)) and 53.22% for the design 3 (Figure 8(b)). Figures 7(a) and 7(b) show the downstream and upstream characteristics of design

ACCEPTED MANUSCRIPT

2(300μm × 300μm) for the three heating power values. The flow induced downstream and upstream sensors shows a resistance change of 18.6% and 15.48% for a power of 55.2mW. The inset of Figure(6b-8b) shows the sensor characteristics in laminar flow regime. It is noteworthy that the heat losses in the laminar flow region is less and it increases as the flow regime shifts to transitional and turbulent.

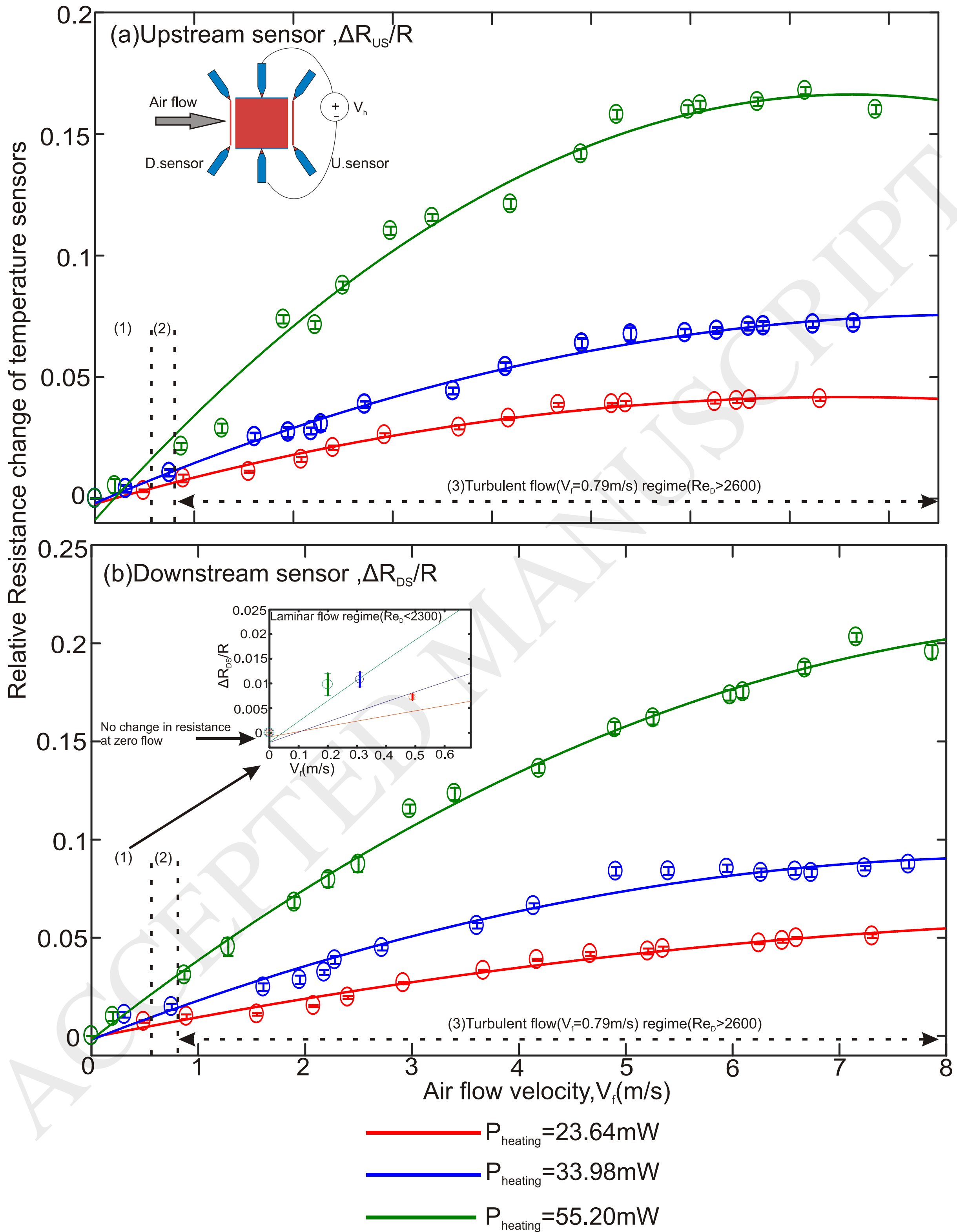

Figure 7. Performance of 300μm×300μm heater with different supplied heating power when the air flow is perpendicular to temperature sensor, **(a)** upstream sensor; **(b)** downstream sensor. Inset of (a) shows the air flow direction and inset of (b) shows the zoomed in response under laminar flow regime.

ACCEPTED MANUSCRIPT

ACCEPTED MANUSCRIPT

Table 2. Performance comparison of our hot film air flow sensor with literature

Heating/sensing material	Substrate material	TCR at (K^{-1})	Relative Resistance change($\Delta R/R$) in%	Sensitivity	References
Platinum	alumina	-	22.08	0.029(s/m)	[55]
Polysilicon	silicon	1100ppm at 100°C	-	$5mV(ms^{-1})^{-0.5}$	[56]
Platinum	silicon	2490ppm at 25°C	-	-	[57]
Carbon Nano tube(CNT)	paper	-750ppm at 25°C	0.8	<0.0016(s/m)	[58]
Graphite	paper	-	2.5	0.0062(s/m)	[59]
Graphite	paper	-2900ppm at 25°C	3.25	0.0081(s/m)	[46]
3C-SiC	glass	-20716ppm at 25°C	58.36	0.091	This work

The sensitivity due to flow is defined as the slope of the output (relative resistance change) characteristics and can be represented mathematically as follows:

$$S = \left(\frac{\Delta R / R}{V_f} \right) = \left(\frac{\frac{R_{\text{flow off}} - R_{\text{flow on}}}{R_{\text{flow off}}}}{V_f} \right) \quad (5)$$

where V_f represents the flow velocity in m/s. The sensitivity of different configurations shown in table 3 were calculated for the turbulent flow regime (Region3 in fig. 6-8) and indicates that downstream sensor is more sensitive than upstream sensor. For instance, the downstream sensor of design 3 (1000μm ×1000μm) (Figure 8(a)) has the highest sensitivity (0.091 s/m), whereas the sensitivity of design 1 (100μm ×100μm) contributes to a mere 7.32×10^{-4}s/m ((Figure 6(a)). Despite the lower sensitivity, the characteristics of the upstream sensor is similar to the downstream sensor. For example, the sensitivity reduces to 6.40×10^{-4}s/m (Figure 6(b)) for the design 1 and 0.079 for the design 3 (Figure 8(b). Figures 7(a) and 7(b) show the sensitivity performances of design 2 (300μm ×300μm) at three applied heating power. The flow induced downstream and upstream sensors show a sensitivity of 0.027s/m and 0.023s/m for a maximum power of 55.20mW. The performance of our SiC hot-film flow sensor is compared with the other hot-film flow sensors based on the relative resistance change(%), TCR and sensitivity(s/m) as shown in table 2.It is to be noted that the comparison was drawn only for air flow sensors which measure sensitivity in s/m. Being a simple, highly sensitive and low power in consumption, our sensor can be employed in various thermal flow sensing applications.

ACCEPTED MANUSCRIPT

Table 3. Performance comparison of the three flow sensor designs under investigation

Heater configuration	100μm×100μm			300μm×300μm			1000μm×1000μm		
Sensing resistor	**Downstream sensor**			**Downstream sensor**			**Downstream sensor**		
Heating power(mW)	P=5.22mW	P=7.98mW	P=13.03mW	P=23.64mW	P=33.98mW	P=55.20mW	P=24.96mW	P=75.47mW	P=133.50mW
Relative change in sensor resistance (%)	0.76	1.3	2.22	4.35	7.65	18.6	5.32	26.35	58.36
Sensitivity(s/m)	7.32×10^{-4}	2.015×10^{-3}	3.32×10^{-3}	6.93×10^{-3}	0.0116	0.027	7.125×10^{-3}	0.039	0.091
Total relative standard error (%)	0.015	0.026	0.030	0.089	0.272	0.457	0.092	0.291	0.528
Sensing resistor	**Upstream sensor**			**Upstream sensor**			**Upstream sensor**		
Heating power(mW)	P=5.22mW	P=7.98mW	P=13.03mW	P=23.64mW	P=33.98mW	P=55.20mW	P=24.96mW	P=75.47mW	P=133.50mW
Relative change in sensor resistance (%)	0.53	1.01	1.72	3.78	6.8	15.48	3.61	24.7	53.22
Sensitivity(s/m)	6.40×10^{-4}	1.36×10^{-3}	2.65×10^{-3}	5.29×10^{-3}	9.98×10^{-3}	0.023	5.86×10^{-3}	0.031	0.079
Total relative standard error (%)	0.013	0.025	0.027	0.059	0.201	0.334	0.090	0.290	0.410

ACCEPTED MANUSCRIPT

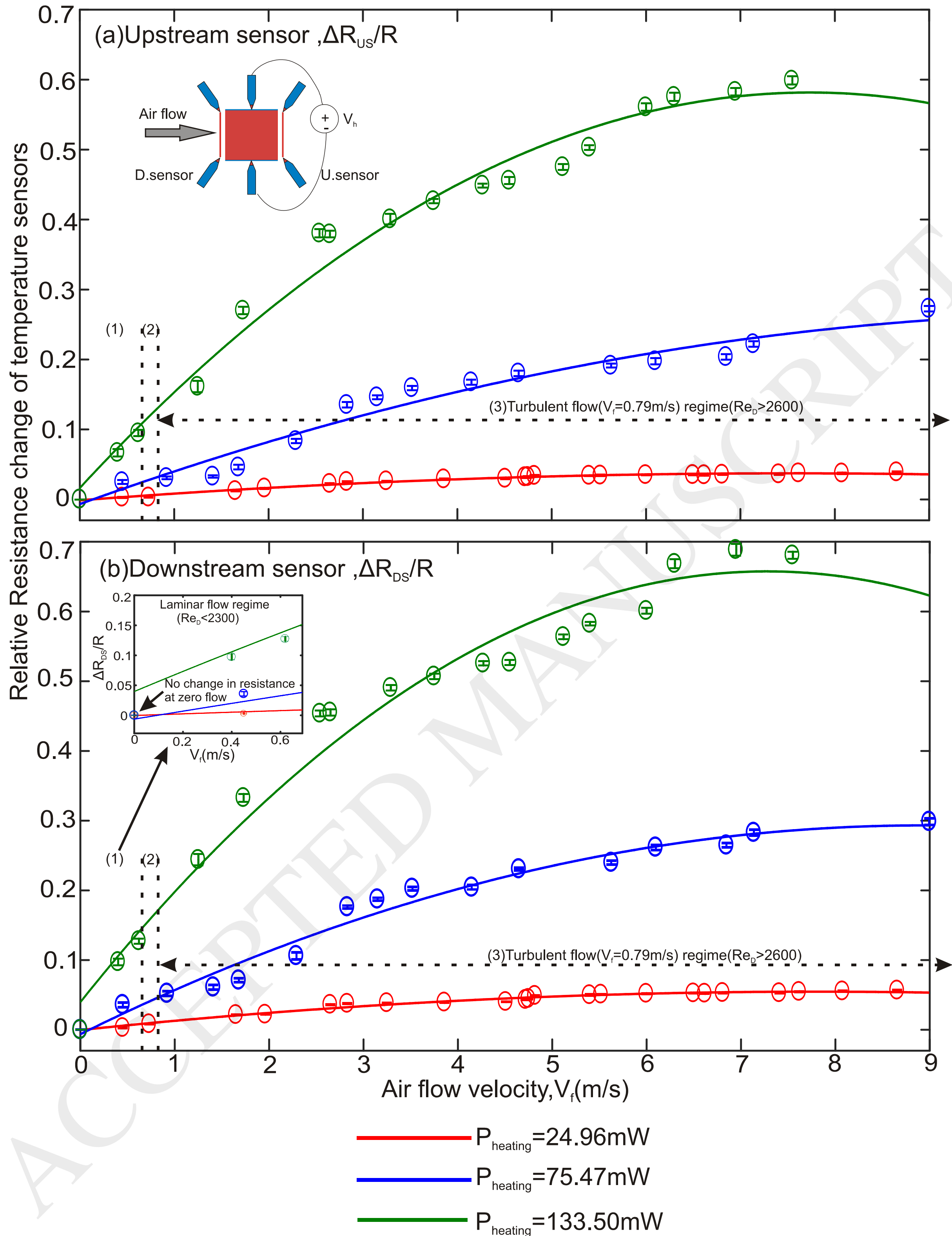

Figure 8. Performance of 1000μm × 1000μm heater with different supplied heating power when the air flow is perpendicular to temperature sensor, **(a)** upstream sensor; **(b)** downstream sensor. Inset of (a) shows the air flow direction and inset of (b) shows the zoomed in response under laminar flow regime.

Finally, the measurement uncertainty (total relative standard error) was calculated to illustrate the errors in the flow measurement. The total relative standard error (TRSE) is expressed as the sum of relative standard error in

ACCEPTED MANUSCRIPT

the absence of the flow and the relative standard error in the presence of the flow. The error bars illustrated in Figures 6 to 8 are too small to be clearly depicted. Table 3 summarizes the aforementioned parameters discussed in this section. We observed that the error percentage tends to increase with the applied heating power and the geometry of the heater respectively.

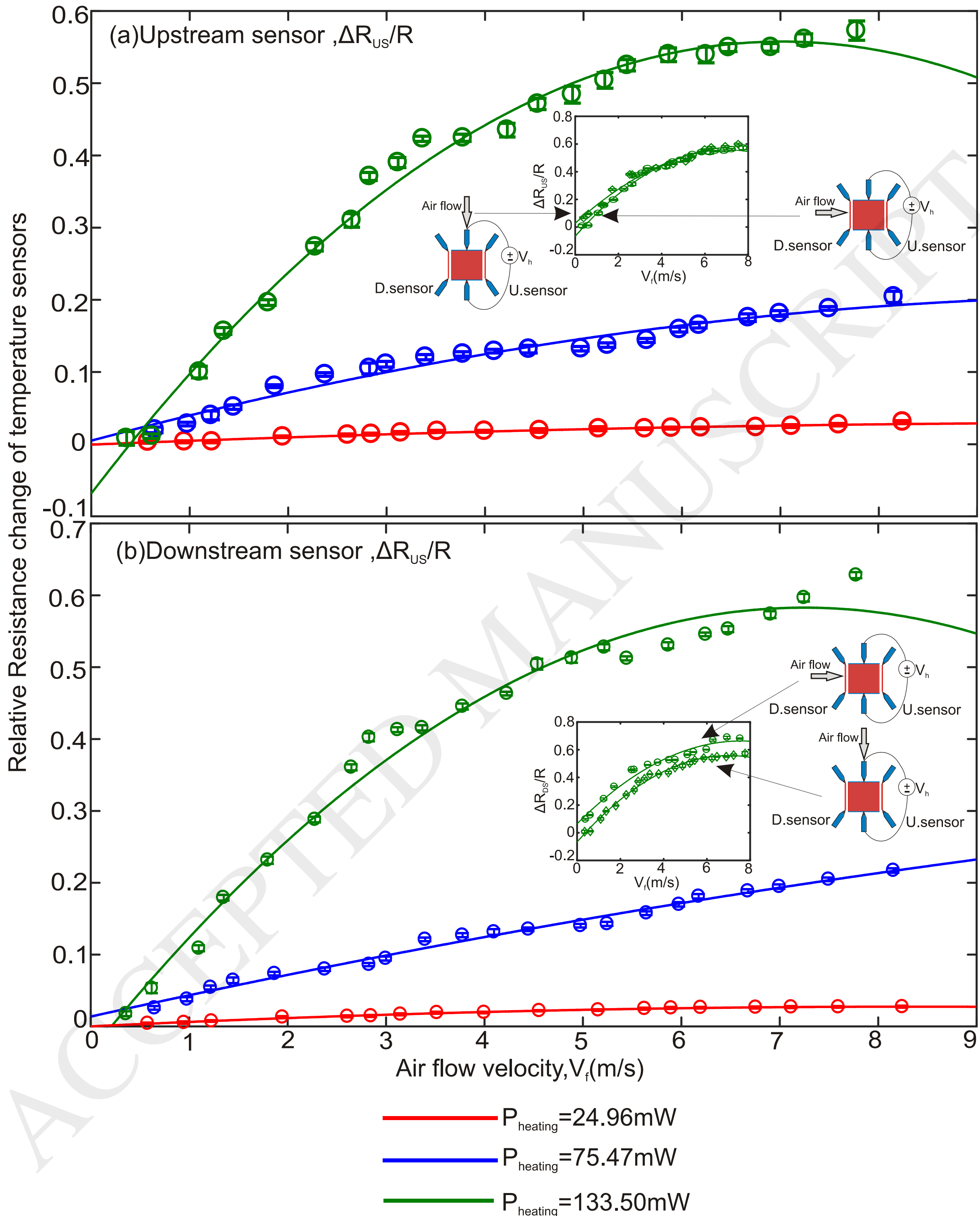

Figure 9. Performance of 1000μm × 1000μm heater at different applied heating power when the air flow is perpendicular to heater, **(a)** upstream sensor; **(b)** downstream sensor. Insets of (a) and (b) show the schematic of flow direction perpendicular to sensor and heater and compare their respective output characteristics.

ACCEPTED MANUSCRIPT

ACCEPTED MANUSCRIPT

Another interesting experiment was conducted to study the influence of flow direction in a thermal sensor. Figure 9(a) and 9(b) shows that the sensor response is less affected by the flow orientation, either perpendicular flow towards the heater or the temperature sensor. That is, the characteristics and the performance of the downstream sensor is better than the upstream sensor as discussed above. However the flow-sensitivity of the sensor is slightly reduced if the flow is perpendicular to the heater. The inset in Figure 9(a) illustrates that air flow normal to the downstream sensor is more sensitive (0.091s/m) than air flow normal to the heater (0.083s/m) in turbulent regime. In a similar way, inset of Figure 9(b) illustrates that air flow normal to upstream sensor is more sensitive (0.079s/m) than air flow normal to the heater (0.072s/m) for a heating power of 133.5mW (blue legend). These results indicate that our flow sensor performs as a hot-film thermal sensor and is relatively independent to flow orientation.

4. Conclusions and future work

We developed a simple and highly sensitive thermal flow sensor for air with 3C-SiC on glass as heating and sensing elements. This SiC layer was transferred to the glass substrate by anodic bonding. The temperature coefficient of resistance (TCR) test showed that n-type SiC exhibits a negative TCR of approximately -20,716ppm/K. The results presented herein, demonstrate that the sensor respond well to air flow over a full range of 0.2 to 9m/s , and requires only several milliwatts to operate. The sensor combines the advantages of small size, low power consumption, high sensitivity and wide dynamic range of flow upto an operating temperature of 170°C. Therefore, we believe that SiC on glass system could potentially meet the demands for low-power and highly sensitive thermal sensors. Future work will involve the fabrication and characterization of suspended SiC thermal structures from the glass substrate which will improve the response time of our flow sensors.Efforts will also be made to develop flow sensors capable of performing in high temperature environments of around and above 500°C.

Acknowledgements

This work was performed in part at the Queensland Node of the Australian National Fabrication Facility, a company established under the National Collaborative Research Infrastructure Strategy to provide nano-and microfabrication facilities for Australia's researchers. The authors acknowledge funding support from Australian Research Council through the ARC linkage grant (LP150100153).

ACCEPTED MANUSCRIPT

ACCEPTED MANUSCRIPT

References

[1] S.O. Kasap, Principles of electronic materials and devices, McGraw-Hill New York, 2006.

[2] J.-P. Colinge, C.A. Colinge, Physics of semiconductor devices, Springer Science & Business Media, 2005.

[3] T. Dinh, H.-P. Phan, T. Kozeki, A. Qamar, T. Fujii, T. Namazu, N.-T. Nguyen, D.V. Dao, High thermosensitivity of silicon nanowires induced by amorphization, Mater. Lett. 177 (2016) 80–84.

[4] N.T. Nguyen, Micromachined flow sensors - a review, Flow Meas. Instrum. 8 (1997) 7–16. doi:10.1016/S0955-5986(97)00019-8.

[5] J.T.W. Kuo, L. Yu, E. Meng, Micromachined thermal flow sensors-A review, Micromachines. 3 (2012) 550–573. doi:10.3390/mi3030550.

[6] V. Balakrishnan, H.-P. Phan, T. Dinh, D.V. Dao, N.-T. Nguyen, Thermal Flow Sensors for Harsh Environments, Sensors. 17 (2017) 2061.

[7] W.-C. Lin, M.A. Burns, Low-power micro-fabricated liquid flow-rate sensor, Anal. Methods. 7 (2015) 3981–3987.

[8] S. Wu, Q. Lin, Y. Yuen, Y.-C. Tai, MEMS flow sensors for nano-fluidic applications, Sensors Actuators A Phys. 89 (2001) 152–158.

[9] A. Feteira, Negative temperature coefficient resistance (NTCR) ceramic thermistors: an industrial perspective, J. Am. Ceram. Soc. 92 (2009) 967–983.

[10] S. Scott, F. Sadeghi, D. Peroulis, An inherently-robust 300 C MEMS temperature sensor for wireless health monitoring of ball and rolling element bearings, in: Sensors, 2009 IEEE, IEEE, 2009: pp. 975–978.

[11] D.C. Abeysinghe, S. Dasgupta, H.E. Jackson, J.T. Boyd, Novel MEMS pressure and temperature sensors fabricated on optical fibers, J. Micromechanics Microengineering. 12 (2002) 229.

[12] J. Bahari, J.D. Jones, A.M. Leung, Sensitivity improvement of micromachined convective accelerometers, J. Microelectromechanical Syst. 21 (2012) 646–655.

[13] J. Bahari, A.M. Leung, Micromachined three-axis thermal accelerometer with a single composite heater, J. Micromechanics Microengineering. 21 (2011) 75025.

[14] V.T. Dau, D.V. Dao, S. Sugiyama, A 2-DOF convective micro accelerometer with a low thermal stress sensing element, Smart Mater. Struct. 16 (2007) 2308.

[15] D.V. Dao, V.T. Dau, T. Shiozawa, S. Sugiyama, Development of a dual-axis convective gyroscope with low thermal-induced stress sensing element, J. Microelectromechanical Syst. 16 (2007) 950–958.

[16] M. Wijesundara, R. Azevedo, Silicon carbide microsystems for harsh environments, Springer Science & Business Media, 2011.

[17] X. Jiang, K. Kim, S. Zhang, J. Johnson, G. Salazar, High-temperature piezoelectric sensing, Sensors. 14 (2013) 144–169.

[18] B. Vivekananathan, L. Ponnusamy, K. Thiruppathi, Design and optimization of multivariable controller for CSTR system, in: Robot. Autom. Control Embed. Syst. (RACE), 2015 Int. Conf., IEEE, 2015: pp. 1–5.

[19] K. Thiruppathi, L. Ponnusamy, B. Vivekananathan, Design and tuning of decoupled PI controllers for real time deep-sea conditions mimicking system, in: Robot. Autom. Control Embed. Syst. (RACE), 2015 Int. Conf., IEEE, 2015: pp. 1–6.

[20] T. Dinh, H.-P. Phan, A. Qamar, P. Woodfield, N.-T. Nguyen, D.V. Dao, Thermoresistive effect for advanced thermal sensors: Fundamentals, design considerations, and applications, J. Microelectromechanical Syst. 26 (2017) 966–986.

[21] J. Spannhake, A. Helwig, G. Müller, T. Doll, SiC as a high-performance material for microheaters, HeT-SiC-05. (2005) 31.

ACCEPTED MANUSCRIPT

ACCEPTED MANUSCRIPT

[22] J. Zhang, C. Carraro, R.T. Howe, R. Maboudian, Electrical, mechanical and metal contact properties of polycrystalline 3C-SiC films for MEMS in harsh environments, Surf. Coatings Technol. 201 (2007) 8893–8898. doi:10.1016/j.surfcoat.2007.05.007.

[23] G.L. Harris, Properties of silicon carbide, Iet, 1995.

[24] J.-G. Lee, M.I. Lei, S.-P. Lee, S. Rajgopal, M. Mehregany, Micro flow sensor using polycrystalline silicon carbide, J. Sens. Sci. Technol. 18 (2009) 147–153.

[25] C. Lyons, A. Friedberger, W. Welser, G. Muller, G. Krotz, R. Kassing, A high-speed mass flow sensor with heated silicon carbide bridges, in: Micro Electro Mech. Syst. 1998. MEMS 98. Proceedings., Elev. Annu. Int. Work., IEEE, 1998: pp. 356–360.

[26] M.I. Lei, Silicon carbide high temperature thermoelectric flow sensor, (2011).

[27] I. Belov, H. Wingbrant, A.L. Spetz, H. Sundgren, B. Thuner, H. Svenningstorp, P. Leisner, Thermal and flow analysis of SiC-based gas sensors for automotive applications, in: Therm. Mech. Simul. Exp. Microelectron. Microsystems, 2004. EuroSimE 2004. Proc. 5th Int. Conf., IEEE, 2004: pp. 475–482.

[28] M. Mehregany, C.A. Zorman, N. Rajan, C.H. Wu, Silicon carbide MEMS for harsh environments, Proc. IEEE. 86 (1998) 1594–1609. doi:10.1109/5.704265.

[29] L. Jiang, R. Cheung, A review of silicon carbide development in MEMS applications, Int. J. Comput. Mater. Sci. Surf. Eng. 2 (2009) 227. doi:10.1504/IJCMSSE.2009.027484.

[30] T. Kimoto, J.A. Cooper, Fundamentals of Silicon Carbide Technology: Growth, Characterization, Devices and Applications, John Wiley & Sons, 2014.

[31] J. Tanaka, A. Jinda, H. Tabuchi, N. Tanaka, H. Furubayashi, Y. Inami, M. Hijikigawa, A micro flow sensor with a substrate having a low thermal conductivity, in: Proceeding 6th Sens. Symp. Inst. Electr. Eng. Japan, Japan, 1986: pp. 125–129.

[32] L. Di Cioccio, Y. Le Tiec, F. Letertre, C. Jaussaud, M. Bruel, Silicon carbide on insulator formation using the Smart Cut process, Electron. Lett. 32 (1996) 1144–1145.

[33] Q. Tong, U. Gösele, C. Yuan, A.J. Steckl, M. Reiche, Silicon carbide wafer bonding, J. Electrochem. Soc. 142 (1995) 232–236.

[34] K.N. Vinod, C.A. Zorman, A.A. Yasseen, M. Mehregany, Fabrication of low defect density 3C-SiC on SiO2 structures using wafer bonding techniques, J. Electron. Mater. 27 (1998) L17–L20.

[35] F. Mu, T. Suga, M. Fujino, Y. Takahashi, H. Nakazawa, K. Iguchi, SiC wafer bonding by modified suface activated bonding method, in: Low Temp. Bond. 3D Integr. (LTB-3D), 2014 4th IEEE Int. Work., IEEE, 2014: p. 55.

[36] H.-P. Phan, H.-H. Cheng, T. Dinh, B. Wood, T.-K. Nguyen, F. Mu, H. Kamble, R. Vadivelu, G. Walker, L. Hold, Single-Crystalline 3C-SiC anodically Bonded onto Glass: An Excellent Platform for High-Temperature Electronics and Bioapplications, ACS Appl. Mater. Interfaces. 9 (2017) 27365–27371.

[37] L. Wang, S. Dimitrijev, J. Han, A. Iacopi, L. Hold, P. Tanner, H.B. Harrison, Growth of 3C–SiC on 150-mm Si (100) substrates by alternating supply epitaxy at 1000 C, Thin Solid Films. 519 (2011) 6443–6446.

[38] S.M. Sze, K.K. Ng, Metal-semiconductor contacts, Wiley Online Library, 2006.

[39] C. Yan, J. Wang, P.S. Lee, Stretchable graphene thermistor with tunable thermal index, ACS Nano. 9 (2015) 2130–2137.

[40] T. Dinh, H.-P. Phan, T.-K. Nguyen, V. Balakrishnan, H.-H. Cheng, L. Hold, A. Lacopi, N.-T. Nguyen, D.V. Dao, Unintentionally doped epitaxial 3C-SiC (111) nanothin film as material for highly sensitive thermal sensors at high temperatures, IEEE Electron Device Lett. 39 (2018) 580–583.

[41] D. Kong, L.T. Le, Y. Li, J.L. Zunino, W. Lee, Temperature-dependent electrical properties of graphene inkjet-printed on flexible materials, Langmuir. 28 (2012) 13467–13472.

[42] F. Warkusz, The size effect and the temperature coefficient of resistance in thin films, J. Phys. D. Appl. Phys. 11 (1978) 689.

ACCEPTED MANUSCRIPT

ACCEPTED MANUSCRIPT

[43] J.S. Shor, D. Goldstein, A.D. Kurtz, Characterization of n-type beta-SiC as a piezoresistor, IEEE Trans. Electron Devices. 40 (1993) 1093–1099.

[44] R.S. Okojie, A.A. Ned, A.D. Kurtz, W.N. Carr, Characterization of highly doped n-and p-type 6H-SiC piezoresistors, IEEE Trans. Electron Devices. 45 (1998) 785–790.

[45] X. Liu, M. Mwangi, X. Li, M. O'Brien, G.M. Whitesides, based piezoresistive MEMS sensors, Lab Chip. 11 (2011) 2189–2196.

[46] T. Dinh, H.-P. Phan, D.V. Dao, P. Woodfield, A. Qamar, N.-T. Nguyen, Graphite on paper as material for sensitive thermoresistive sensors, J. Mater. Chem. C. 3 (2015) 8776–8779.

[47] H. Al-Mumen, F. Rao, L. Dong, W. Li, Design, fabrication, and characterization of graphene thermistor, in: Nano/Micro Eng. Mol. Syst. (NEMS), 2013 8th IEEE Int. Conf., IEEE, 2013: pp. 1135–1138.

[48] A. Di Bartolomeo, M. Sarno, F. Giubileo, C. Altavilla, L. Iemmo, S. Piano, F. Bobba, M. Longobardi, A. Scarfato, D. Sannino, Multiwalled carbon nanotube films as small-sized temperature sensors, J. Appl. Phys. 105 (2009) 64518.

[49] V. Balakrishnan, T. Dinh, H.-P. Phan, D.V. Dao, N.-T. Nguyen, A generalized analytical model for Joule heating of segmented wires, J. Heat Transfer. 140 (2018) 72001.

[50] V. Balakrishnan, T. Dinh, H.-P. Phan, T. Kozeki, T. Namazu, D.V. Dao, N.-T. Nguyen, Steady-state analytical model of suspended p-type 3C–SiC bridges under consideration of Joule heating, J. Micromechanics Microengineering. 27 (2017) 75008.

[51] F. Mailly, A. Giani, R. Bonnot, P. Temple-Boyer, F. Pascal-Delannoy, A. Foucaran, A. Boyer, Anemometer with hot platinum thin film, Sensors Actuators A Phys. 94 (2001) 32–38. doi:http://dx.doi.org/10.1016/S0924-4247(01)00668-9.

[52] C. Sosna, T. Walter, W. Lang, Response time of thermal flow sensors, Procedia Eng. 5 (2010) 524–527.

[53] C.-P. Wang, C.-W. Liu, C. Gau, Silicon nanowire temperature sensor and its characteristic, in: Nano/Micro Eng. Mol. Syst. (NEMS), 2011 IEEE Int. Conf., IEEE, 2011: pp. 630–633.

[54] A. Bosseboeuf, P.E. Allain, F. Parrain, X. Le Roux, N. Isac, S. Jacob, A. Poizat, P. Coste, S. Maaroufi, A. Walther, Thermal and electromechanical characterization of top-down fabricated p-type silicon nanowires, Adv. Nat. Sci. Nanosci. Nanotechnol. 6 (2015) 25001.

[55] R.-H. Ma, Y.-H. Wang, S.-L. Chiang, C.-Y. Lee, Fabrication and characterization of MEMS-based flow sensors based on hot films, Microsyst. Technol. 17 (2011) 655–660.

[56] T. Neda, K. Nakamura, T. Takumi, A polysilicon flow sensor for gas flow meters, Sensors Actuators A Phys. 54 (1996) 626–631.

[57] S.-T. Hung, S.-C. Wong, W. Fang, The development and application of microthermal sensors with a mesh-membrane supporting structure, Sensors Actuators A Phys. 84 (2000) 70–75.

[58] T. Dinh, H.-P. Phan, T.-K. Nguyen, A. Qamar, A.R.M. Foisal, T.N. Viet, C.-D. Tran, Y. Zhu, N.-T. Nguyen, D.V. Dao, Environment-friendly carbon nanotube based flexible electronics for noninvasive and wearable healthcare, J. Mater. Chem. C. 4 (2016) 10061–10068.

[59] T. Dinh, H.-P. Phan, T.-K. Nguyen, A. Qamar, P. Woodfield, Y. Zhu, N.-T. Nguyen, D.V. Dao, Solvent-free fabrication of biodegradable hot-film flow sensor for noninvasive respiratory monitoring, J. Phys. D. Appl. Phys. 50 (2017) 215401.

ACCEPTED MANUSCRIPT

ACCEPTED MANUSCRIPT

Author biographies

Mr. Vivekananthan Balakrishnan is currently a PhD student at the Queensland Micro-and Nanotechnology Centre, Griffith University, Australia. He received his BE degree from Anna University, Trichy and ME degree in Control and Instrumentation Engineering from College of Engineering, Guindy, India in 2013 and 2015, respectively. His current research focus is the design, optimisation and characterisation of SiC thermal sensors. His research interests also include microelectronics, control system design and process control. He is a recipient of the Griffith University Postgraduate Research Scholarship (GUPRS) and the International Postgraduate Research Scholarship (IPRS).

Dr Toan Dinh received his B.E. and M.Sc. degrees from Hanoi University of Science and Technology, Vietnam, in 2009 and 2012, respectively. He was awarded his PhD from Griffith University in 2017. He is currently a Research Fellow at Queensland Micro- and Nanotechnology Centre, Griffith University. His research interests include micro/nano-electromechanical systems (MEMS/NEMS), physics of semiconductors and sensors for harsh environments, soft robotics and advanced functional materials for wearable applications. He was a recipient of GUPRS, IPRS and Publication Assistance Scholarship (PAS) from Griffith University.

Dr. Hoang-Phuong Phan (B.E and M.E. the University of Tokyo, Japan; Ph.D. Griffith University, Australia) is currently a research fellow at the Queensland Micro and Nanotechnology Centre, Griffith University, where his main interests focus on silicon carbide MEMS/NEMS for applications in harsh environments. He has also been a visiting scholar at the National Institute of Advanced Industrial Science and Technology (AIST), Japan in 2016, and Stanford University, CA, US in 2017. Dr. Phan has published more than 50 peer-reviewed journal articles and conference papers, two US patents, and one book, all in micro and nanotechnologies. He was the recipient of the Japanese Government Scholarships (MEXT) for undergraduate and postgraduate studies (2006-2013), and the GUPRS and GUIPRS scholarships from Griffith University for the doctoral course (2013-2016). Dr. Phan was honoured with the PAS award, the GGRS-IEIS travel grant, the Springer outstanding theses award, the Australian Nanotechnology Network Overseas Fellowship, and the Griffith University Postdoctoral Fellowship. He was also selected to the Australian delegates to attend the 23rd World Micromachines Summit in Barcelona, Spain in 2017. Dr. Phan has served as a reviewer for several journals, including JMEMS, Sensors and Actuators A, Micro machines, Material Science & Engineering B, IEEE Sensors Journal, IEEE Electron Device Letters, and Journal of Applied Physics.

Dr Dzung Viet Dao received his PhD degree in Micro Electro Mechanical Systems (MEMS) from Ritsumeikan University, Japan in 2003. He served as a Postdoctoral Research Fellow from 2003 to 2006, Lecturer from 2006 to 2007, and Chair Professor from 2007 to 2011, all at Ritsumeikan University, Japan. From 2011 Dr Dao joined Griffith University as a Senior Lecturer in the School of Engineering, where he is currently teaching Mechatronics and Mechanical Engineering. Dr Dao current research interests include nanostructures, MEMS sensors & actuators, silicon carbide transducers for harsh environment, and mechatronics. Dr Dao has published over 270 papers in scientific journals and conference proceedings, and filed 15 Japanese patents.

Prof. Nam-Trung Nguyen is a professor and the director of Queensland Micro- and Nanotechnology Centre, Griffith University, Australia. He received his Dipl-Ing, Dr-Ing and Dr-Ing Habil degrees from the Chemnitz University of Technology, Germany, in 1993, 1997 and 2004, respectively. He was a postdoctoral research engineer at the Berkeley Sensor and Actuator Center, University of California, Berkeley, USA. From 1999 to 2013 he was a research fellow, assistant professor and associate professor at Nanyang Technological University, Singapore. Dr. Nguyen has published over 330 journal papers and several books on microfluidics and nanofluidics.

ACCEPTED MANUSCRIPT

Accepted Manuscript

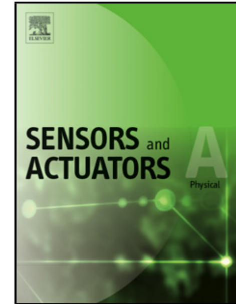

Title: Highly Sensitive 3C-SiC on glass based thermal flow sensor realized using MEMS technology

Authors: Vivekananthan Balakrishnan, Toan Dinh, Hoang-Phuong Phan, Dzung Viet Dao, Nam-Trung Nguyen

PII: S0924-4247(18)30163-8
DOI: https://doi.org/10.1016/j.sna.2018.06.025
Reference: SNA 10830

To appear in: *Sensors and Actuators A*

Received date: 26-1-2018
Revised date: 8-6-2018
Accepted date: 11-6-2018

Please cite this article as: Balakrishnan V, Dinh T, Phan H-Phuong, Dao DV, Nguyen N-Trung, Highly Sensitive 3C-SiC on glass based thermal flow sensor realized using MEMS technology, *Sensors and Actuators: A. Physical* (2018), https://doi.org/10.1016/j.sna.2018.06.025

This is a PDF file of an unedited manuscript that has been accepted for publication. As a service to our customers we are providing this early version of the manuscript. The manuscript will undergo copyediting, typesetting, and review of the resulting proof before it is published in its final form. Please note that during the production process errors may be discovered which could affect the content, and all legal disclaimers that apply to the journal pertain.